Indian Journal of Chemical Technology
Vol. 29, November, 2022 pp. 616-634
DOI: 10.56042/ijct.v29i6.67406

Molecular docking and computational studies investigation on a bioactive anti-cancer drug: Thiazole derivatives

A Viji*[,1], R Vijayakumar[2], V Balachandran[3], K Vanasundari[3] & M Janaki[1]

[1]Department of Physics, Kongunadu College of Engineering & Technology, Thottiyam Tiruchirappalli 621 215, Tamil Nadu, India

[2]PG and Research Department of Physics, Srimad Andavan Arts and Science College, (Affiliated to Bharathidasan University) Tiruchirappalli 620 005, Tamil Nadu, India

[3]Department of Physics, Arignar Anna Government Arts College, Musiri, (Affiliated to Bharathidasan University) Tiruchirappalli 621 211, Tamil Nadu, India.

E-mail: vijiarangarasan@gmail.com

Received 19 August 2022; accepted 21 October 2022

In the present work, the 1-Benzyl-3-[2-(3-(4-chlorophenyl)-5-[4-(propan-2-yl)phenyl]-4,5-dihydro-1*H*-pyrazol-1-yl)-4-oxo-4,5-dihydro-1,3-thiazol-5(4*H*)-ylidene]-2,3-dihydro-1*H*-indol-2-one (BCPOT) anticancer candidates to treatment of breast cancer based on B3LYP level 6-31G(d,p) and LanL2DZ basis sets calculations and molecular docking. BCPOT have been proposed as potential stabilization energies, and topological properties have been evaluated as a function of acceptors and donor groups present in their structures. Detailed interpretation of the vibrational spectral assignments has been carried out using the Potential energy distribution (PED) analysis. The evaluation of the Fukui functions has also been carried out to describe the activity of the sites in the title compound. The non-covalent interaction (NCI) of the molecule has been explained by a reduced density gradient. Molecular electrostatic potential explains the nucleophilic and electrophilic reaction of the molecule. Molecular orbital interaction has been explained by Frontier molecular orbitals. For a better prediction of the anticancer properties of the proposed compound, molecular docking calculations are performed by using four structures of breast cancer activity. Docking results have been discussed based on binding affinities and the interaction types among ligands and different amino acid residues, indicating the powerful ability of ligands in front of the novel cancer disease.

Keywords: Thiazole, Anticancer, Molecular docking, Computational studies

In this work, structures of compounds clinically used as anticancer drugs for the treatment of abundant infections including their activity spectral, mechanisms of action, major indications, and administration have been carefully studied by Clerk[1]. Therefore, biologically those compounds are known while only some of them the structural, electronic, topological, and vibrational properties were studied combining experimental results with theoretical calculations derived from the density functional theory (DFT)[2]. This work has the purpose of proposing BCPOT compounds for the treatment of breast cancer based on some important properties predicted by computational DFT calculations and specific molecular docking studies. High-resolution crystal structures of the enzyme from three viral serotypes have been used for the design. Anticancer therapeutics with profiles of high potency, low resistance, and low toxicity remain challenging, and obtaining such agents continues to be an active area of therapeutic development. Due to their unique three-dimensional structural features, BCPOT has been identified as one of the privileged chemotypes of anticancer drug development. Thiazole and its derivatives are very useful compounds in different fields of chemistry including medicine and agriculture. Thiazoles, for instance, exhibit widespread biological activities like antiviral, anti-diabetic, antibacterial, anticancer, and antifungal[3,4]. The present work describes the Quantum chemical calculation of 1-Benzyl-3-[2-(3-(4-chlorophenyl)-5-[4-(propan-2-yl)phenyl]-4,5-dihydro-1*H*-pyrazol-1-yl)-4-oxo-4,5-dihydro-1,3-thiazol-5(4*H*)-ylidene]-2,3-dihydro-1*H*-indol-2-one (BCPOT) by density functional theory. The redistribution of electron density in various bonding and antibonding orbitals along with stabilization energies have been calculated by natural bond orbital analysis to give clear proof of stabilization originating from hyper-conjugation of a variety of intra-molecular interactions.

The Mulliken atomic charges and Fukui functions have been analyzed. Molecular docking is a powerful computational tool in predicting the binding affinity of a ligand with the proteins, which is very much useful and effective in modern structure-based drug designing. The structure of the target protein can be obtained from the protein data bank (PDB) format. The ligand-protein molecular docking can predict the preferred orientation of the ligand concerning the protein to form a stable complex and its derivatives.

Experimental Section

The compound was synthesized by refluxing 3-(4-chlorophenyl)-5-[4-propan-2-yl)phenyl]-4,5-dihydro-1*H*-pyrazole-1-carbothioamide(0.01 mol) and 2-(bromomethyl)-4-methoxyphenol (0.01 mol in ethanol/DMF mixture (30 mL) as per the procedure reported by Vinutha *et al.*[5]. Fourier transform infrared (FT-IR) spectrum of the compound was recorded employing the Perkin-Elmer spectrometer fitted with a KBr beam splitter around 4000-450 cm^{-1}. Bruker RFS 27 FT-Raman spectrometer was used to report the FT-Raman spectrum in the region 4000-0 cm^{-1} using a 1064 nm Nd: YAG laser source. Both spectral measurements were performed at the Sophisticated Analytical Instrumentation Facility (SAIF), IIT, Madras, India.

Computational details

All the calculations of the title compound were carried out using Gaussian 09 software[6] by utilizing Becke's three-parameter hybrid model with the Lee-Yang-Parr correlation functional (B3LYP) method. The LANL2DZ and 6-31G(d,p) basis set was employed to predict the molecular structure and vibrational wavenumbers. Gauss View program was used for the visualization of optimized structures[7]. Molecular electrostatic potentials and Natural population analysis were also computed at the same level. The non-covalent interactions were studied and their reduced density gradient was graphed by Multiwfn[8]. Molecular docking studies were performed with the help of Autodock software[9].

Results and Discussion

Molecular geometry

The geometry of the molecule under investigation is considered by possessing C_1 point group symmetry. The optimized molecular structure of BCPOT along with the numbering of the atom is shown in Fig. 1. To understand the vibrational frequencies, it is essential to know the geometry of the compound. The values of the optimized bond lengths and bond angles of

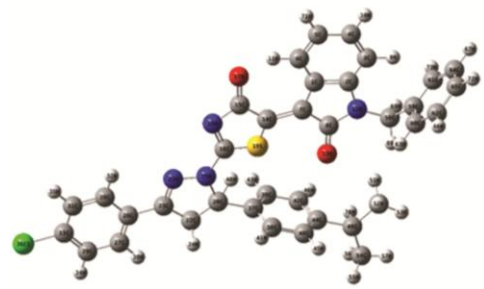

Fig. 1 — Optimized molecular structure of BCPOT

BCPOT are presented in Tables 1 and 2. Generally, the carbon-carbon bonds in phenyl ring are not the same length. The bonds C1-C2 = 1.45/1.42, C1-C6 = 1.38/1.40, C1-C7 = 1.46/1.46, C2-C3 = 1.38/1.39, C3-C4 = 1.40/1.40, C4-C5 = 1.39/1.40, C5-C6 = 1.40/1.40, C7-C8 = 1.41/1.50, C7-C15 = 1.54/1.54, C8-C14 = 1.43/1.23, C15-C16 = 1.40/1.22, C15-C20 = 1.39/1.39, C22-C26 = 1.39/1.09, C26-C49 = 1.29/1.39, C27-C28 = 1.40/1.09, C27-C29 = 1.39/1.39, C28-C31 = 1.10/1.39, C29-C33 = 1.10/1.40, C38-C39 = 1.40/1.09, C38-C40 = 1.39/1.40, C39-C42 = 1.10/1.40, C40-C44 = 1.10/1.40, C59-C60 = 1.54/1.40, C60-C61 = 1.40/1.09, C60-C62 = 1.39/1.40, C61-C64 = 1.10/1.40, C62-C65 = 1.40/1.09 are varied. The C-H bond lengths of BCPOT are fall in C3-H9 = 1.10/1.08, C4-H10 = 1.10/1.09, C5-H11 = 1.10/1.09, C22-H24 = 1.39/1.52, C23-H24 = 1.40/1.10, C23-H48 = 1.07/1.40, C28-H30 = 1.39/1.08, C29-H32 = 1.40/1.08, C39-H41 = 1.39/1.09, C40-H43 = 1.40/1.09, C50-H51 = 1.54/1.09, C50-H55 = 1.54/1.10, C50-H71 = 1.07/1.10, C59-H69 = 1.07/1.40, C59-H70 = 1.07/1.39 Å, C61-H63 = 1.39/1.09 Å, C65-H66 = 1.39/1.40 Å, C65-H68 = 1.10/1.20 Å, H66-H72 = 1.07/1.05 Å which is in good agreement with the reported values[10]. The calculated shorter bond length is O_{25}-H_{26} =0.96 Å and the longer bond length is Cl_{11}-O_{24}=2.07 Å. Ergodu *et al.*[11] reported that the optimized bond angles of C-C-C and C-N-C in phenyl ring fall in the range from 119°-120°. In the present case, these angles fall in C1-C2-C3, C4-C3-H9, C5-C4-H10, C4-C5-H11, C5-C6-N12, H24-C27-C28, H24-C27-C29, C28-C27-C29, C27-C28-H30, C27-C28-C31, H30-C28-C31, C27-C29-H32, C27-C29-C33, C28-H30-H35, H34-H30-H35, C29-H32-Cl36, N21-C38-C39, C39-C38-C40, C38-C39-H41, C38-C39-C42, C38-C40-H43, C38-C40-C44, C39-H41-H46, C61-C60-C62, C60-C61-C64, H63-C61-C64, C60-C62-C65, C60-C62-H73, C65-C62-H73, C61-H63-H66, C61-H63-H67, H66-H63-

Table 1 — Optimized geometrical parameter (bond lengths(Å)) of 1-benzyl-3-[2-(3-(4-chlorophenyl)-5-[4-(propan-2-yl)phenyl]-4,5-dihydro-1*H*-pyrazol-1-yl)-4-oxo-4,5-dihydro-1,3-thiazol-5(4*H*)-ylidene]-2,3-dihydro-1*H*-indol-2-one obtained B3LYP/ lanl2dz and B3LYP/6-31G (d, p) basis sets.

Parameters	Bond lengths (Å)		Parameters	Bond lengths (Å)		Parameters	Bond lengths (Å)	
	B3LYP/ lanl2dz	B3LYP/6-31G(d,p)		B3LYP/ lanl2dz	B3LYP/ 6-31G(d,p)		B3LYP/ lanl2dz	B3LYP/6-31G(d,p)
C1-C2	1.45	1.42	N21-C49	1.08	1.38	H45-C50	1.54	1.10
C1-C6	1.38	1.40	C22-H24	1.39	1.52	C50-H51	1.54	1.09
C1-C7	1.46	1.46	C22-C26	1.39	1.09	C50-H55	1.54	1.10
C2-C3	1.38	1.39	C23-H24	1.40	1.10	C50-H71	1.07	1.10
C2-O13	1.46	1.40	C23-N25	1.07	1.46	H51-H52	1.07	1.10
C3-C4	1.40	1.40	C23-H48	1.07	1.40	H51-H53	1.07	1.09
C3-H9	1.10	1.08	H24-C27	1.54	1.41	H51-C54	1.07	1.10
C4-C5	1.39	1.40	C26-C49	1.29	1.39	H55-H56	1.07	1.52
C4-H10	1.10	1.09	C27-C28	1.40	1.09	H55-H57	1.07	1.10
C5-C6	1.40	1.40	C27-C29	1.39	1.39	H55-C58	1.07	1.09
C5-H11	1.10	1.09	C28-H30	1.39	1.08	C59-C60	1.54	1.40
C6-N12	1.10	1.08	C28-C31	1.10	1.39	C59-H69	1.07	1.40
C7-C8	1.41	1.50	C29-H32	1.40	1.08	C59-H70	1.07	1.39
C7-C15	1.54	1.54	C29-C33	1.10	1.40	C60-C61	1.40	1.09
C8-O13	1.41	1.38	H30-H34	1.40	1.08	C60-C62	1.39	1.40
C8-C14	1.43	1.23	H30-H35	1.10	1.76	C61-H63	1.39	1.09
H9-C62	2.10	1.46	H32-H34	1.39	1.40	C61-C64	1.10	1.40
N12-N18	1.65	1.52	H32-Cl36	1.10	1.40	C62-C65	1.40	1.09
O13-C59	1.47	1.77	H34-C37	1.76	1.39	C62-H73	1.07	1.39
C15-C16	1.40	1.22	C38-C39	1.40	1.09	H63-H66	1.40	1.09
C15-C20	1.39	1.39	C38-C40	1.39	1.40	H63-H67	1.10	1.09
C16-N18	1.43	1.30	C39-H41	1.39	1.09	C65-H66	1.39	1.40
C16-S19	1.43	1.81	C39-C42	1.10	1.40	C65-H68	1.10	1.20
O17-S19	1.40	1.35	C40-H43	1.40	1.09	H66-H72	1.07	1.05
O17-C20	1.39	1.55	C40-C44	1.10	1.40			
O17-C26	1.54	1.49	H41-H45	1.40	1.09			
N21-C23	1.43	1.52	H41-H46	1.10	1.52			
N21-C26	1.40	1.09	H43-H45	1.39	1.54			
N21-C38	1.54	1.29	H43-H47	1.10	1.54			

Table 2 — Optimized geometrical bond angles(degrees) of 1-Benzyl-3-[2-(3-(4-chlorophenyl)-5-[4-(propan-2-yl)phenyl]-4,5-dihydro-1*H*-pyrazol-1-yl)-4-oxo-4,5-dihydro-1,3-thiazol-5(4*H*)-ylidene]-2,3-dihydro-1*H*-indol-2-one obtained B3LYP/ lanl2dz and B3LYP/6-31G (d, p) basis sets.

Parameters	Bond angle (degree)		Parameters	Bond angle (degree)		Parameters	Bond angle (degree)	
	B3LYP/ lanl2dz	B3LYP/6-31G(d,p)		B3LYP/ lanl2dz	B3LYP/6-31G(d,p)		B3LYP/ lanl2dz	B3LYP/6-31G(d,p)
C2-C1-C7	107	107	H24-C23-N25	110	112	H43-H45-C50	120	112
C6-C1-C7	133	134	H24-C23-H48	110	113	H45-C50-H51	120	112
C1-C2-C3	120	122	N25-C23-H48	110	111	H45-C50-H55	120	107
C1-C2-O13	107	110	C22-H24-C23	108	108	H45-C50-H71	90	111
C3-C2-O13	133	128	C22-H24-C27	121	114	H51-C50-H55	120	107
C2-C3-C4	118	118	C23-H24-C27	130	121	H51-C50-H71	90	
C2-C3-H9	121	121	O17-C26-N21	130	125	H55-C50-H71	90	111
C4-C3-H9	120	121	O17-C26-C22	121	127	C50-H51-H52	109	111
C3-C4-C5	121	121	O17-C26-C49	118	120	C50-H51-H53	109	111
C3-C4-H10	119	119	N21-C26-C22	108	113	C50-H51-C54	109	108
C5-C4-H10	120	120	C22-C26-C49	145	121	H52-H51-H53	109	108
C4-C5-C6	121	121	H24-C27-C28	120	120	H52-H51-C54	109	108

(*Contd*.)

Table 2 — Optimized geometrical bond angles(degrees) of 1-Benzyl-3-[2-(3-(4-chlorophenyl)-5-[4-(propan-2-yl)phenyl]-4,5-dihydro-1*H*-pyrazol-1-yl)-4-oxo-4,5-dihydro-1,3-thiazol-5(4*H*)-ylidene]-2,3-dihydro-1*H*-indol-2-one obtained B3LYP/ lanl2dz and B3LYP/6-31G (d, p) basis sets. (*Contd.*)

Parameters	Bond angle (degree)		Parameters	Bond angle (degree)		Parameters	Bond angle (degree)	
	B3LYP/ lanl2dz	B3LYP/6-31G(d,p)		B3LYP/ lanl2dz	B3LYP/6-31G(d,p)		B3LYP/ lanl2dz	B3LYP/6-31G(d,p)
C4-C5-H11	120	120	H24-C27-C29	120	119	H53-H51-C54	109	111
C6-C5-H11	119	119	C28-C27-C29	120	121	C50-H55-H56	109	111
C1-C6-C5	118	119	C27-C28-H30	120	120	C50-H55-H57	109	111
C1-C6-N12	121	119	C27-C28-C31	120	119	C50-H55-C58	109	108
C5-C6-N12	120	121	H30-C28-C31	120	121	H56-H55-H57	109	108
C1-C7-C8	108	106	C27-C29-H32	120	119	H56-H55-C58	109	108
C1-C7-C15	125	135	C27-C29-C33	120	120	H57-H55-C58	109	114
C8-C7-C15	127	119	H32-C29-C33	120	119	O13-C59-C60	109	109
C7-C8-O13	110	107	C28-H30-H34	120	121	O13-C59-H69	109	105
C7-C8-C14	125	127	C28-H30-H35	120	120	O13-C59-H70	109	110
O13-C8-C14	125	125	H34-H30-H35	120	119	C60-C59-H69	109	110
C2-O13-C8	108	110	C29-H32-H34	120	121	C60-C59-H70	109	108
C2-O13-C59	125	127	C29-H32-Cl36	120	120	H69-C59-H70	109	120
C8-O13-C59	127	123	H34-H32-Cl36	120	121	C59-C60-C61	120	121
C7-C15-C16	130	128	H30-H34-H32	120	119	C59-C60-C62	120	119
C7-C15-C20	121	122	H30-H34-C37	120	119	C61-C60-C62	120	120
C16-C15-C20	108	109	H32-H34-C37	120	121	C60-C61-H63	120	119
C15-C16-N18	126	123	N21-C38-C39	120	120	C60-C61-C64	120	120
C15-C16-S19	107	113	N21-C38-C40	120	119	H63-C61-C64	120	121
N18-C16-S19	126	124	C39-C38-C40	120	120	C60-C62-C65	120	120
S19-O17-C20	108	119	C38-C39-H41	120	120	C60-C62-H73	120	120
S19-O17-C26	130	124	C38-C39-C42	120	120	C65-C62-H73	120	120
C20-O17-C26	121	117	H41-C39-C42	120	121	C61-H63-H66	120	120
C16-S19-O17	107	112	C38-C40-H43	120	120	C61-H63-H67	120	120
C15-C20-O17	109	87	C38-C40-C44	120	120	H66-H63-H67	120	120
C23-N21-C26	107	101	H43-C40-C44	120	121	C62-C65-H66	120	120
C23-N21-C38	126	114	C39-H41-H45	120	119	C62-C65-H68	120	120
C23-N21-C49	151	111	C39-H41-H46	120	120	H66-C65-H68	120	120
C26-N21-C38	126	113	H45-H41-H46	120	121	H63-H66-C65	120	120
C38-N21-C49	71	109	C40-H43-H45	120	119	H63-H66-H72	120	120
H24-C22-C26	109	109	C40-H43-H47	120	119	C65-H66-H72	120	120
N21-C23-H24	107	109	H45-H43-H47	120	118			
N21-C23-N25	110	102	H41-H45-H43	120	121			

H67, C62-C65-H66, C62-C65-H68, H66-C65-H68, H63-H66-C65, H63-H66-H72, C65-H66-H72=120^0. For BCPOT, the shorter and longer bond angles are H51-C50-H71 = 90°/107, C6-C1-C7 = 133°/134°. The greater bond angles are assigned to be due to the delocalization of electrons due to the presence of the phenyl ring.

Vibrational spectral analysis

The title compound 1-Benzyl-3-[2-(3-(4-chlorophenyl)-5-[4-(propan-2-yl)phenyl]-4,5-dihydro-1*H*-pyrazol-1-yl)-4-oxo-4,5-dihydro-1,3-thiazol-5(4*H*)-ylidene]-2,3-dihydro-1*H*-indol-2-one (BCPOT) comprises of 73 atoms, giving rise to 213 vibrational modes. Vibrational assignments have been carried out for the complete span of wavenumbers predicted theoretically with the DFT method. Minor divergences are observed between the theoretical and experimental values. The experimental FT-IR and FT-Raman spectra for the title compound are shown in Figs 2 and 3 along with the theoretical ones. Table 3 shows the complete vibrational assignments based on the percentage PED values along the experimental and theoretical results.

Aromatic compounds commonly exhibit multiple weak bands in the region 3100-3000 cm^{-1} (Ref.12) due to aromatic C-H stretching vibrations. Accordingly, in the present study the C-H stretching vibrations of BCPOT is Calculated wave numbers at 3113, 3108,

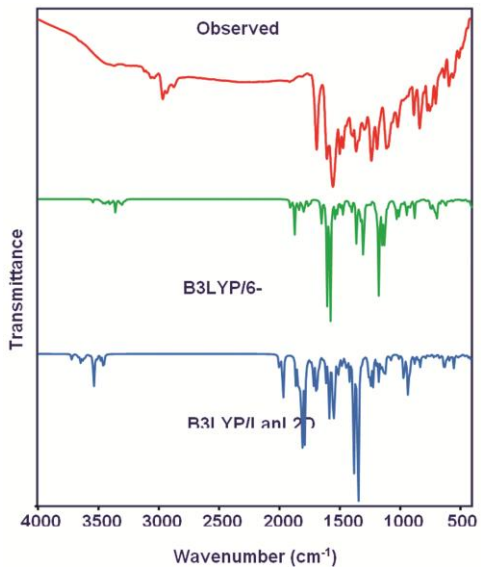

Fig. 2 — Observed FT-IR and simulated spectra of BCPOT.

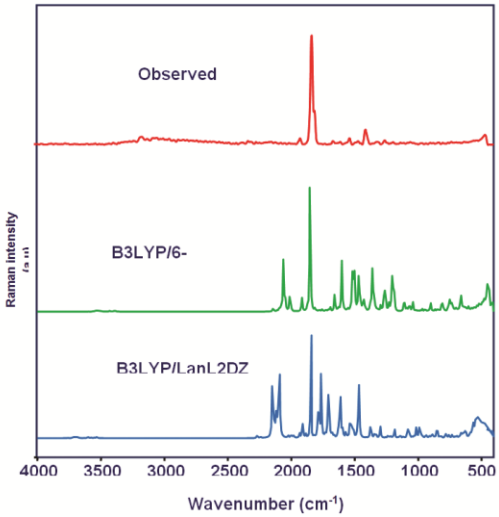

Fig. 3 — Observed FT-Raman and simulated spectra of BCPOT.

3101, 3095, 3092, 3088, 3086, 3076, 3071, 3064, 3060, 3055, 3049, 3044, 3040, 3035, 3026, 2968, 2934 [LanL2DZ] and 3110, 3105, 3098, 3093, 3089, 3085, 3079, 3072, 3067, 3061, 3056, 3052, 3045, 3041, 3036, 3031, 3021, 2966, 2930 cm^{-1} [6-31G (d, p)]. Corresponding experimental vibrations are identified at 3111vw, 3057vw, 3032vw (FT-IR) and 3063w cm^{-1} (FT-Raman). The bands due to C-H in-plane and out-of-plane bending vibration interacting somewhat with C-C stretching vibration are observed as several medium weak intensity sharp bands in the region 1300-1000 cm^{-1} and 1000-750 cm^{-1} (Ref.13). In BCPOT, the C-H in-plane bending vibrations are observed at 1547ms, 1491w (FT-IR), and 1550ms cm^{-1} (FT-Raman) respectively. The computed values by B3LYP/ LanL2DZ method are predicted at 1550, 1537, 1512, 1495, 1483, 1380, 1375, 1370, 1154, 1150, 1145, 1133, 1125 cm^{-1} and by B3LYP/6-31G (d, p) 1548, 1535, 1512, 1493, 1482, 1376, 1373, 1369, 1154, 1149, 1140, 1131, 1124 cm^{-1}. Theoretical spectrum obtained at 971, 965, 958, 950, 949, 944, 938, 935, 923, 919, 880, 875, 869, 862, 859, 845, 811, 798 cm^{-1} B3LYP/ LanL2DZ and by B3LYP/6-31G (d, p) are 968, 963, 957, 951, 945, 940, 936, 931, 923, 917, 879, 875, 866, 860, 857, 845, 808, 796 identified as CH out-of-plane bending vibrations.

The CC stretching vibrations in the aromatic ring are generally observed at 1600-1460 cm^{-1} (Ref.14). In the present case, carbon-carbon stretching vibrations are assigned at 1597vw, 1287vw, 1228ms, 1181vw, 1010w cm^{-1} (FT-IR) and 1584vs, 1179vw, 1062vw, 1011vw cm^{-1} (FT-Raman). The computed values by B3LYP/ LanL2DZ method are predicted at 1615, 1607, 1600, 1590, 1585, 1581, 1575, 1565, 1340, 1330, 1322, 1305, 1290, 1228, 1182, 1097, 1075, 1061, 1050, 1018, 1005, 997, 989, 984, 980, 976, 905, 896, 840, 793, 784, 778, 764 cm^{-1} and by B3LYP/6-31G (d, p) 1613, 1605, 1599, 1588, 1583, 1579, 1574, 1562, 1338, 1329, 1320, 1302, 1288, 1226, 1180, 1095, 1072, 1060, 1047, 1015, 1003, 995, 988, 982, 979, 974, 902, 894, 838, 790, 782, 775, 762 cm^{-1}.

The methylene group (CH_2) of the title molecule which works as a bridge between the COOH group and phenyl ring, shows the CH_2 asymmetric stretching, symmetric stretching, scissoring, rocking, wagging, and twisting vibrational modes. The asymmetric and symmetric C-H stretching vibrations of CH_2 appear in the range 2936-2916 cm^{-1} and 2865-2845 cm^{-1} respectively[15]. The CH_2 asymmetric stretching mode calculated wavenumbers are 3015, 2993 cm^{-1} (LanL2DZ) and 3013, 2990 (6-31G (d, P)). The CH_2 scissoring vibrations appear normally in the region 1490-1435 cm^{-1} as a medium intense band[16]. In the present case, The CH_2 scissoring mode is found to be strongly mixed with the CH_2 scissoring modes of the phenyl ring, and the dominant CH_2 scissoring mode is assigned at 1466, 1450 cm^{-1} (LanL2DZ), and 1465, 1447 (6-31G (d, P)) with experimental FTIR band at 1464w cm^{-1}. CH_2 wagging mode is calculated at 1207, 1165, and 1206, 1163 which is in good agreement with an observed band at 1162 vw cm^{-1} in the FT-IR spectrum. The dominant mode corresponding to the CH_2 rocking vibrational motions are assigned at 1366, 1354, and 1364, 1354 cm^{-1},

Table 3 — Observed and calculated FT-IR and FT-Raman frequencies for 1-Benzyl-3-[2-(3-(4-chlorophenyl)-5-[4-(propan-2-yl)phenyl]-4,5-dihydro-1*H*-pyrazol-1-yl)-4-oxo-4,5-dihydro-1,3-thiazol-5(4*H*)-ylidene]-2,3-dihydro-1*H*-indol-2-one obtained B3LYP/ lanl2dz and B3LYP/6-31G (d, p) basis sets.

S. No.	Observed wavenumbers (cm^{-1})		Calculated wavenumbers (cm-1)		Vibrational assignments (%PED)
	FT-IR	FT-Raman	B3LYP/ LAN12DZ	B3LYP/ 6-31G(d,p)	
1	3111vw		3113	3110	ν CH (99)
2			3108	3105	ν CH (98)
3			3101	3098	ν CH (98)
4			3095	3093	ν CH (99)
5			3092	3089	ν CH (97)
6			3088	3085	ν CH (98)
7			3086	3079	ν CH (98)
8			3076	3072	ν CH (97)
9		3063w	3071	3067	ν CH (99)
10	3057vw		3064	3061	ν CH (99)
11			3060	3056	ν CH (99)
12			3055	3052	ν CH (98)
13			3049	3045	ν CH (98)
14			3044	3041	ν CH (97)
15			3040	3036	ν CH (97)
16	3032vw		3035	3031	ν CH (98)
17			3026	3021	ν CH (98)
18			3015	3013	ν_{ass} CH_2 (97)
19	3032vw		3006	3004	ν_{ass} CH_3 (97)
20			2998	2996	ν_{ass} CH_3 (98)
21			2993	2990	ν_{ass} CH_2 (98)
22			2985	2982	ν_{ass} CH_3 (97)
23			2976	2975	ν_{ass} CH_3 (97)
24			2968	2966	ν CH (98)
25			2964	2961	ν_{ss} CH_2 (97)
26	2962vw		2956	2954	ν_{ss} CH_2 (97)
27			2948	2945	ν_{ss} CH_3 (98)
28		2929vw	2941	2938	ν_{ss} CH_3 (98)
29	1682vs		2934	2930	ν CH (97)
30			1636	1633	ν CO (75), ν CN (17)
31			1625	1624	ν CO (72), ν CN (18)
32			1615	1613	ν CC (78),δ CH(17)
33			1607	1605	ν CC (75),δ CH(20)
34	1597w		1600	1599	ν CC (75),δ CH(18)
35			1597	1594	ν CN (65), ν CC (20),δ CH(10)
36			1590	1588	ν CC (68),δ CH(26)
37		1584vs	1585	1583	ν CC (68),δ CH(26)
38			1581	1579	ν CC (68),δ CH(25)
39			1575	1574	ν CC (75), ν CN (16)
40			1570	1569	ν CN (70), ν CC (15)
41			1565	1562	ν CC (83),δ CH(11)
42			1557	1555	ν CN (66), ν CC (20),δ CH(10)
43	1547ms	1550ms	1550	1548	δ CH(80), ν CC (11)
44			1537	1535	δ CH(81), ν CH (12)
45			1524	1523	δ_{opb} CH_3 (72)
46			1512	1512	δ CH(68)

(*Contd.*)

Table 3 — Observed and calculated FT-IR and FT-Raman frequencies for 1-Benzyl-3-[2-(3-(4-chlorophenyl)-5-[4-(propan-2-yl)phenyl]-4,5-dihydro-1*H*-pyrazol-1-yl)-4-oxo-4,5-dihydro-1,3-thiazol-5(4*H*)-ylidene]-2,3-dihydro-1*H*-indol-2-one obtained B3LYP/ lanl2dz and B3LYP/6-31G (d, p) basis sets. (*Contd*.)

S. No.	Observed wavenumbers (cm^{-1})		Calculated wavenumbers (cm-1)		Vibrational assignments (%PED)
	FT-IR	FT-Raman	B3LYP/ LAN12DZ	B3LYP/ 6-31G(d,p)	
47			1503	1500	δ_{opb} CH_3 (75)
48	1491w		1495	1493	δ CH(66), ν CC (12)
49			1483	1482	δ CH(68), ν CC (12)
50		1475vw	1478	1476	δ_{ipb} CH_3 (72)
51			1474	1470	δ_{ipb} CH_3 (68)
52	1464w		1466	1465	σ_{Sci} CH_2 (78)
53			1450	1447	σ_{Sci} CH_2 (78)
54	1436vw		1437	1435	ν CN(63), ν CC (20)
55			1416	1415	ν CN(62), ν CC (22)
56		1398vw	1400	1399	δ_{Sb} CH_3 (65), ν CC (12)
57	1382vw		1386	1383	ν CN (62), ν NN (20)
58			1380	1376	δ CH(63), ν CC (21)
59			1375	1373	δ CH(66), ν CC (18)
60			1370	1369	δ CH(63), ν CC (18)
61			1366	1364	ρ_{rock} CH_2 (63), ν CN (16)
62			1360	1359	δ_{Sb} CH_3 (69), ν CC (15)
63	1355w		1354	1354	ρ_{rock} CH_2 (64), ν CN (16)
64			1340	1338	ν CC (61), δ CH(15)
65			1330	1329	ν CC (61), δ CH(18)
66			1322	1320	ν CC (60), ρ_{rock} CH_2 (19)
67		1312vw	1316	1314	ν CN (60), ρ_{rock} CH_2 (18)
68			1305	1302	ν CC (58), ρ_{rock} CH_2 (18)
69			1298	1297	γ CH(60), δ CC (20)
70	1287vw		1290	1288	ν CC (62), δ CC(18)
71			1280	1279	δ CH(58), ν CC (26)
72			1273	1273	δ CN(58), ν CC (25)
73			1270	1268	δ CN(58), ν CC (26)
74			1263	1262	δ CH(60), ν CC (18)
75		1254w	1258	1255	δ CH(61), ν CC (22)
76	1491w		1244	1241	δ CH(62), ν CC (20)
77	1228ms		1228	1226	ν CC (55), δ CH(18)
78			1207	1206	σ_{wag} CH_2 (55), γ CH(12)
79			1190	1188	δ CO(52), ν CC (21), ν CN (10)
80	1181vw	1179vw	1182	1180	ν CC (60), δ CH(12)
81			1173	1172	γ CH(58), ν CC (19)
82			1170	1168	δ CO(55), ν CN (20)
83		1162vw	1165	1163	σ_{wag} CH_2 (50), γ CH(18)
84			1154	1154	δ CH(60), δ CC (19), δ CCl (10)
85			1150	1149	δ CH(60), δ CC (18), δ CCl (12)
86			1145	1140	δ CH(51), ν CC (19), ν CO (12)
87			1133	1131	δ CH(50), ν CC (19), ν CO (10)
88			1125	1124	δ CH(50), ν CC (21), ν CCl (12)
89		1115ms	1118	1116	τ CH_2(58)
90			1113	1109	τ CH_2(60)
91	1103w		1107	1105	γ CO(58)
92			1100	1099	γ CO(57)
93			1097	1095	ν CC (54),δ CH(20)
94	1089ms		1090	1090	ν NN (57),δ CN(18)
95			1075	1072	ν CC (52),δ CH(18)

(*Contd*.)

Table 3 — Observed and calculated FT-IR and FT-Raman frequencies for 1-Benzyl-3-[2-(3-(4-chlorophenyl)-5-[4-(propan-2-yl)phenyl]-4,5-dihydro-1*H*-pyrazol-1-yl)-4-oxo-4,5-dihydro-1,3-thiazol-5(4*H*)-ylidene]-2,3-dihydro-1*H*-indol-2-one obtained B3LYP/ lanl2dz and B3LYP/6-31G (d, p) basis sets. (*Contd.*)

S. No.	Observed wavenumbers (cm^{-1})		Calculated wavenumbers (cm-1)		Vibrational assignments (%PED)
	FT-IR	FT-Raman	B3LYP/ LAN12DZ	B3LYP/ 6-31G(d,p)	
96		1062vw	1061	1060	ν CC (54),δ CH(21)
97	1010w	1011vw	1050	1047	ν CC (54),δ CH(19)
98			1018	1015	ν CC (52), δ_{sb} CH_3(20)
99			1013	1010	δ_{ipr} CH_3(54)
100			1005	1003	ν CC (54),δ CH(17)
101			997	995	ν CC (54),δ CH(18)
102			989	988	ν CC (54),δ_{sciss} CH_2(20)
103			984	982	ν CC (54),δ_{sciss} CH_2 (22)
104			980	979	ν CC (52),δ CCl(18)
105			976	974	ν CC (56)
106			971	968	γ CH(57), σ_{wagg} CH_2 (24)
107			965	963	γ CH(54), σ_{wagg} CH_2 (25)
108			958	957	γ CH(52), σ_{wagg} (26)
109		948vw	950	951	γ CH(50), σ_{wagg} (25)
110			949	945	γ CH(50)
111			944	940	γ CH(51)
112			938	936	γ CH(50)
113			935	931	γ CH(48), γ_{opr} CH_3(17)
114			930	928	δ_{ipr} CH_3(56), δ CH(24)
115			923	923	γ CH(50), γ_{opr} CH_3(14)
116			919	917	γ CH(51), $\sigma_{wagg}$$CH_2$ (17)
117		900vw	911	910	γ_{opr} CH_3(49)
118			905	902	ν CC (54),δ CH(18)
119			896	894	ν CC (53),δ CH(18)
120			893	890	ν CN (60),δ CO(20)
121			885	883	γ_{opr} CH_3(55)
122			880	879	γ CH(50), γ CO(18)
123	876ms	874vw	875	875	γ CH(50), γ CO(18)
124			869	866	γ CH(51), γ CO(18)
125			862	860	γ CH(50), γ CC(22)
126			859	857	γ CH(51), γ CC(18)
127			845	845	γ CH(50), γ CC(20)
128			840	838	ν CC (58), $\sigma_{sciss}$$CH_2$(18)
129	828w	825vw	825	822	ν CCl (58)
130			817	815	ν CCL (55), δ CH (17)
131			811	808	γ CH(50)
132			798	796	γ CH(52)
133			793	790	ν CC (55),δ CH(22)
134		781vw	784	782	ν CC (55),δ CH(20)
135			778	775	ν CC (55),δ CH(22)
136	764vw		764	762	ν CC (55),δ CH(22)
137			753	750	δ CC(55), δ CH(20)
138	744vw		745	742	δ CC(54), δ CH(20)
139			738	736	δ_{ring}(60)
140			732	730	δ CC(54), δ CCl(21)
141		724vw	726	722	δ CC(52), δ CCl(21)
142			715	712	δ_{ring}(66)
143			705	704	δ CC(53), δ CH(25)
144	695w		694	692	δ CC(55), δ CH(20)

(*Contd.*)

Table 3 — Observed and calculated FT-IR and FT-Raman frequencies for 1-Benzyl-3-[2-(3-(4-chlorophenyl)-5-[4-(propan-2-yl)phenyl]-4,5-dihydro-1*H*-pyrazol-1-yl)-4-oxo-4,5-dihydro-1,3-thiazol-5(4*H*)-ylidene]-2,3-dihydro-1*H*-indol-2-one obtained B3LYP/ lanl2dz and B3LYP/6-31G (d, p) basis sets. (*Contd*.)

S. No.	Observed wavenumbers (cm^{-1})		Calculated wavenumbers (cm-1)		Vibrational assignments (%PED)
	FT-IR	FT-Raman	B3LYP/ LAN12DZ	B3LYP/ 6-31G(d,p)	
145			675	673	δ_{ring}(64)
146		662vw	663	660	δ_{ring}(65)
147			648	644	δ_{ring}(66)
148			641	639	δ_{ring}(66)
149	624vw	625vw	626	625	ν CS (59),δ CN(18)
150			618	615	ν CS (58),δ CO(18)
151		600vw	605	603	γ CC(48), γ CH(22)
152			595	592	δ CCl(55), δ CH(20)
153	585vw		590	586	δ_{ring}(60)
154			582	579	δ CC(53)
155			670	568	δ CC(53)
156		562vw	564	561	γ CC(50), γ CH(20)
157	550vw		556	552	γ CC(48), γ CC(22)
158		537vw	540	538	γ CC(48), γ CC(20)
159			515	512	δ_{ring}(65)
160	501w		504	503	γ CC(48), γ CH(22)
161			494	492	δ_{ring}(60)
162			485	484	δ_{ring}(64)
163		475vw	480	476	δ_{ring}(60)
164			465	463	δ_{ring}(61)
165	450vw		453	452	δ_{ring}(60)
166			440	438	γ_{ring} (51)
167			423	420	γ_{ring} (50)
168			413	411	γ_{ring} (51)
169			404	401	γ_{ring} (50)
170			400	396	γ_{ring} (54)
171			391	388	δ_{ring}(56)
172		375vw	375	373	δ_{ring}(56)
173			355	351	γ_{ring} (54)
174			343	338	γ_{ring} (52)
175			328	325	γ_{ring} (54)
176			316	312	δ_{ring}(55)
177			310	306	δ_{ring}(53)
178			298	294	γ_{ring} (54)
179			287	285	δ_{ring}(55)
180			280	277	γ_{ring} (54)
181			274	269	γ_{ring} (55)
182			263	261	δ_{ring}(54)
183		250vw	254	250	γ_{ring} (51)
184			239	235	γ_{ring} (50)
185			225	221	δ_{ring}(52)
186			216	212	γ_{ring} (50)
187			209	206	δ_{ring}(56)
188			195	193	γ_{ring} (52)
189			189	188	δ_{ring}(56)
190			166	165	δ_{ring}(55)
191			160	158	γ CCl(55), γ CH(19)
192		150vw	153	151	δ_{ring}(66)
193			137	136	δ_{ring}(64)

(*Contd*.)

Table 3 — Observed and calculated FT-IR and FT-Raman frequencies for 1-Benzyl-3-[2-(3-(4-chlorophenyl)-5-[4-(propan-2-yl)phenyl]-4,5-dihydro-1*H*-pyrazol-1-yl)-4-oxo-4,5-dihydro-1,3-thiazol-5(4*H*)-ylidene]-2,3-dihydro-1*H*-indol-2-one obtained B3LYP/ lanl2dz and B3LYP/6-31G (d, p) basis sets. (*Contd*.)

194		133	130	δ_{ring}(64)
195		121	119	δ_{ring}(65)
196		115	112	γ_{ring} (60)
197		104	101	γ_{ring} (54)
198		95	92	γ_{ring} (55)
199		80	76	γ_{ring} (58)
200		73	70	γ_{ring} (58)
201	74vw	65	64	γ_{ring} (55)
202		58	56	γ_{ring} (55)
203		49	45	γ_{ring} (57)
204		46	40	γ_{ring} (57)
205		42	39	τ CH_3(55)
206		35	34	τ CH_3(55)
207		34	31	γ_{ring} (49)
208		28	26	γ_{ring} (50)
209		25	22	γ_{ring} (50)
210		19	14	γ_{ring} (50)
211		17	14	γ_{ring} (49)
212		13	10	γ_{ring} (41)
213		8	6	γ_{ring} (49)

respectively, and in good agreement with experimental data (1355w cm^{-1} in FTIR).

The absorption bands arising from C-N symmetric stretching modes are observed in the wavenumber region 1150-850 cm^{-1} (Refs 17,18). In the present case, C-N stretching vibrations are assigned at 1436vw, 1382vw cm^{-1} (FT-IR), and 1312vw cm^{-1} (FT-Raman). The calculated spectrum of LanL2DZ and 6-31G (d, P) at 1597, 1570, 1557, 1437, 1416, 1386, 1316, 893 and 1594, 1569, 1555, 1435, 1415, 1383, 1314, 890 cm^{-1} are assigned to the C-N stretching mode of BCPOT.

The vibrational mode belonging to the bond between the ring and halogen atom is worth discussing here since the mixing of vibrations is possible due to the lowering of the molecular symmetry and the presence of a heavy atom on the periphery of the molecule[19]. The C-Cl absorption is observed in the broad region between 750-580 cm^{-1} (Ref.20). Thus, the band observed in the IR spectrum at 828w cm^{-1} and FT-Raman at 825vw cm^{-1} is assigned to the C-Cl stretching mode of BCPOT. The C-Cl in-plane bending mode is 595 cm^{-1} LanL2DZ and 592 cm^{-1} 6-31G (d, p). The calculated value of C-Cl out-of-plane bending is computed at 160 (LanL2DZ), 158 cm^{-1} (6-31G (d, p)).

The stretching vibration assigned to the C–S linkage occurs in the range of 700–600 cm^{-1} (Ref.21). The bands were identified at 644, 459 cm^{-1} (IR), 640, 480 cm^{-1} (Raman), and 650, 473, and 267 cm^{-1} theoretically for C-S vibrations assigned by Maha *et al*.[22]. In the present case, C-S stretching vibrations are assigned at 624vw cm^{-1} (FT-IR) and 625vw cm^{-1} (FT-Raman). The calculated spectrum of LanL2DZ and 6-31G (d, P) at 626, 618, and 625, 615 cm^{-1} are assigned to the C-S stretching mode of BCPOT.

The thiazole and phenyl ring in-plane bending vibrations were calculated at 738, 715, 675, 663, 648, 641, 590, 515, 494, 485, 480, 465, 453, 391, 375, 316, 310, 287, 263, 225, 209, 189, 166, 153, 137, 133, 121 cm^{-1} for B3LYP/ LanL2DZ and 736, 712, 673, 660, 644, 639, 586, 512, 492, 484, 476, 463, 452, 388, 373, 312, 306, 285, 261, 221, 206, 188, 165, 151, 136, 130, 119 cm^{-1} B3LYP/6-31G (d, p). The peak was observed at 585vw, 450vw cm^{-1} in FT-IR, and 662vw, 475vw, 375vw, and 150vw cm^{-1} in the FT-Raman spectrum was assigned to ring in-plane bending vibration. The ring out-of-plane bending vibrations were calculated at 440, 423, 413, 404, 400, 355, 343, 328, 298, 280, 274, 254, 239, 216, 195, 115, 104, 95, 80, 73, 65, 58, 49, 46, 34, 28, 25, 19, 17, 13, 8 cm^{-1} for B3LYP/ LanL2DZ and 438, 420, 411, 401, 396, 351, 338, 325, 294, 277, 269, 250, 235, 212, 193, 112, 101, 92, 76, 70, 64, 56, 45, 40, 31, 26, 22, 16, 14, 10, 6 cm^{-1} B3LYP/6-31G(d, p). The observed values are at 250vw, and 74vw cm^{-1} in the FT-Raman spectrum. The group and skeletal deformational modes were calculated at the low wavenumber region.

Charge analysis

The charge distribution on a molecule has a significant influence on the vibrational spectra. The atomic charge in molecules is fundamental to chemistry. For instance, the atomic charge has been describing the process of electro negativity equalization and charge transfer in chemical reactions[23,24]. Mulliken atomic charges and natural atomic charges are computed by the DFT/B3LYP method 6-31G (d, p) basis set. The computed reactive atomic charges play an important role in the application of quantum mechanical calculations of the molecular system. The charges of the title compound are tabulated in Table 4 and shown in Fig. 4. The results show that substitution of the phenyl ring by chlorine atoms leads to redistribution of electron density. The charges of CH_2 groups are the same distribution. Hydrogen atoms H9, H10, H11, H24, H30, H32, H34, H35, H41, H43, H45, H46, H47, H48, H51, H52, H53, H55, H56, H57, H63, H66, H67, H68, H69, H71, H72 and H73 exhibit a positive charge (0.2 a.u), S19 = 0.913/0.801 a.u which is an acceptor atom. Oxygen (O_{13}= -0.398 /-0.706 a.u, O17 = -0.400/-0.655 a.u) have high negative charge, which are donor atoms.

Molecular electrostatic potential (MEP)

Molecular electrostatic potential (MEP) gives a clear picture of the distribution of charge at the surface and surrounding of the title compound in three dimensions. By doing so, the nature of interactions and chemical bonds can be identified. Colour grading helps us to classify nucleophilic and electrophilic

Table 4 — Natural and Mulliken atomic charge of 1-Benzyl-3-[2-(3-(4-chlorophenyl)-5-[4-(propan-2-yl)phenyl]-4, 5-dihydro-1*H*-pyrazol-1-yl)-4-oxo-4,5-dihydro-1,3-thiazol-5(4*H*)-ylidene]-2,3-dihydro-1*H*-indol-2-one

Atoms numbers	Mulliken charge (a.u)	Natural charge (a.u)	Atoms numbers	Mulliken charge (a.u)	Natural charge (a.u)
C1	0.159	-0.094	C38	-0.295	-0.168
C2	0.212	0.197	C39	-0.344	-0.181
C3	-0.219	-0.255	C40	-0.385	-0.181
C4	-0.262	-0.177	H41	0.236	0.228
C5	-0.314	-0.226	C42	-0.393	-0.202
C6	-0.312	-0.149	H43	0.235	0.228
C7	0.231	-0.033	C44	0.500	0.024
C8	0.012	0.614	H45	0.234	0.228
C9	0.241	0.226	H46	0.227	0.226
H10	0.212	0.219	H47	0.263	0.248
H11	0.354	0.282	H48	0.205	0.430
N12	-0.237	-0.476	C49	-0.103	-0.225
O13	-0.398	-0.706	C50	-0.672	-0.614
C14	-0.485	-0.429	H51	0.218	0.219
C15	0.013	0.559	H52	0.216	0.214
C16	-0.390	0.051	H53	0.200	0.209
O17	-0.400	-0.655	C54	-0.691	-0.614
N18	-0.059	-0.559	H55	0.210	0.206
S19	0.913	0.801	H56	0.209	0.209
C20	-0.010	-0.108	H57	0.216	0.218
N21	-0.050	-0.228	C58	-0.475	-0.198
C22	-0.569	-0.498	C59	0.433	-0.029
C23	0.077	0.281	C60	-0.338	-0.210
H24	0.257	0.244	C61	-0.447	-0.246
N25	-0.216	-0.247	C62	-0.223	-0.200
C26	0.376	-0.088	H63	0.234	0.227
C27	-0.359	-0.200	C64	-0.216	-0.205
C28	-0.348	-0.165	C65	-0.233	-0.213
C29	-0.213	-0.221	H66	0.217	0.224
H30	0.233	0.225	H67	0.217	0.223
C31	-0.207	-0.219	H68	0.228	0.216
H32	0.283	0.258	H69	0.239	0.242
C33	-0.110	-0.012	H70	0.149	0.223
H34	0.245	0.242	H71	0.235	0.219
H35	0.251	0.245	H72	0.267	0.223
Cl36	-0.034	-0.017	H73	0.234	0.217
C37	0.312	-0.094			

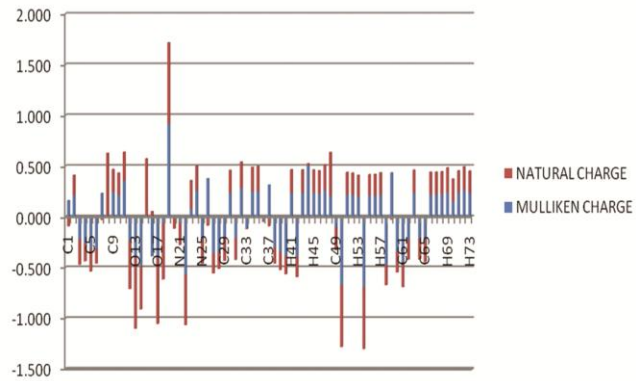

Fig. 4 — Graphical representation of charge analysis of BCPOT.

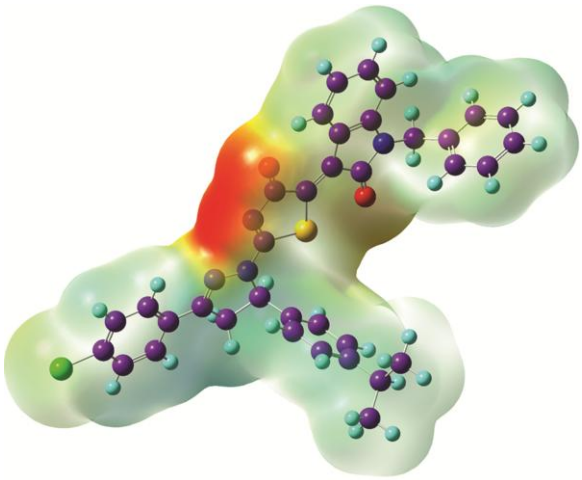

Fig. 5 — Molecular electrostatic potential of BCPOT.

regions effortlessly. It also aids in evaluating the physiochemical properties of the title compound[25].

Figure 5 shows the MEP map for the title compound. A scale ranging from -8.840×10^{-2} a.u to 8.840×10^{-2} a.u with colour grading (Red<Orange< Yellow<Green<Blue in the potential increasing order) is used. O atom has the highest electrophilicity indicated by the red colour, while hydrogen atoms have the highest nucleophilicity. Neutral regions are shown in green.

HOMO – LUMO analysis

Knowledge of the highest occupied molecular orbital (HOMO) and lowest unoccupied molecular orbital (LUMO) and their properties such as their energy is very useful to gauge the chemical reactivity of the molecule. The ability of the molecule to donate an electron is associated with the HOMO and the characteristic of the LUMO is associated with the molecule's electron affinity. The HOMO and LUMO energies are very useful for physicists and chemists and are very important terms in quantum chemistry[26].

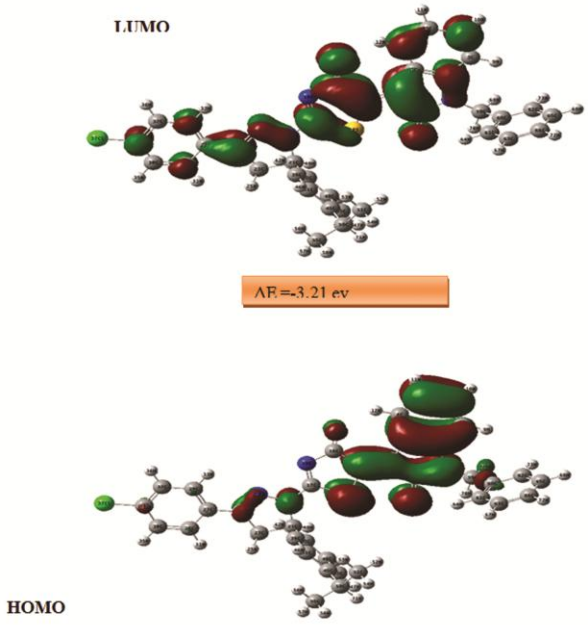

Fig. 6 — HOMO LUMO energy gap of BCPOT.

In the present study, the HOMO and LUMO energies have been predicted at the B3LYP method with a 6-31G (d,p) basis set. According to the calculated results, the energy value of HOMO is computed as -5.68eV and the energy of LUMO is -2.47eV. As a result, a very small energy gap observed between HOMO and LUMO is -3.21 eV. The distribution and energy levels of the HOMO-LUMO orbital of BCPOT are shown in Fig. 6.

The positive phase is red and the negative one is green. The chemical hardness and softness of a molecule are a good standards to value the chemical stability of a molecule. The chemical hardness and softness of a molecule depend on the energy gap between HOMO-LUMO. The molecules having a small energy gap are known as soft molecules and molecules having a large energy gap are known as hard molecules. The soft molecules are more polarizable than the hard ones due to their need for small energy for excitation. BCPOT has a small energy gap, hence from the calculation, it can be concluded that the molecule taken for investigation belongs to soft material. The lowering of the HOMO-LUMO band gap is essentially a consequence of the large stabilization of the LUMO due to the strong electron accepting ability of the electron acceptor group[27]. The energies of HOMO and LUMO and their neighboring orbitals are all negative values, which indicates BCPOT is stable[28].

Local reactivity descriptors

Fukui function is one of the broadly used local density functional descriptors to represent the chemical reactivity and site selectivity of the molecule. It is local reactivity descriptors that specify the selected regions where a chemical species will modify its density when the quantity of the electron was changed[29]. It is feasible to describe the equivalent condensed or aromatic Fukui functions on the kth atom site as stated in the below equations (1-3):

$$f_k^+ = q_k (N+1) - q_k (N) \quad \ldots (1)$$

$$f_k^- = q_k (N) - q_k (N-1) \quad \ldots (2)$$

$$f_k^0 = ½ \{q_k (N+1) - q_k (N-1)\} \quad \ldots (3)$$

f_k^+indicates the molecule under nucleophilic and f_k^- indicates the electrophilic attack.

In the above equation, q_k is the atomic charge at the k^{th}atomic site is the neutral (N), anionic (N+1), or cationic (N-1) chemical species. Morell*et al.*[30] proposed a dual descriptor Δf(r), which is defined as the difference between the nucleophilic and electrophilic Fukui function and is given by

$$\Delta f(r) = [f+(r) - f-(r)] \quad \ldots (4)$$

Δf(r)>0, then the site is favoured for a nucleophilic attack whereas if Δf(r)<0, then the site is favored for an electrophilic attack, and these values are summarized in Table 5. The behaviour of molecules as electrophiles (C2 = -0.108, C7 = -0.002, C8 = -0.327, H9 = -0.120, H10 = -0.117, H11 = -0.141, C15 = -0.283, C16 = -0.023, S19 = -0.399, C20 = -0.141, C23 = -0.279, H24 = -0.167, N25 = -0.011, H30 = -0.117, H32 = -0.133, C33= -0.026, H34 = -0.129, H35 = -0.131, Cl = -0.017, H41 = -0.116, H43 = -0.116, C44 = -0.024, H45 = -0.120, H46 = -0.118, H47 = -0.165, H48 = -0.240, H51 = -0.108, H52 = -0.106, H53 = -0.110, H55 = -0.105, H56 = -0.106, H57 = -0.113, H63 = -0.112, H66 = -0.115, H67 = -0.116, H68 = -0.113, H69 = -0.123, H70 = -0.112, H71 = -0.114, H72 = -0.113, H73 = -0.115) or nucleophiles (C1 = 0.052, C3 = 0.122, C4 = 0.067, C5 = 0.107, C6 = 0.062, N12 = 0.235, O13 = 0.316, C14 = 0.170, O17 = 0.273, N18 = 0.253, N21 = 0.145, C22 = 0.267, C26 = 0.064, C27 = 0.066, C28 = 0.056, C29 = 0.112, C31 = 0.108, C37 = 0.059, C38 = 0.069, C39 = 0.084, C40 = 0.087, C42 = 0.099, C49 = 0.114, C50 = 0.306, C54 = 0.306, C58 = 0.099, C59 = 0.022, C60 = 0.107, C61 = 0.124, C62 = 0.097, H64 = 0.100, H65 = 0.101) during reaction depends on the local behavior of molecules.

NBO analysis

In quantum chemistry, a natural bond orbital (NBO) is a computed bonding orbital with maximum electron density. Natural bond orbitals are used in computational chemistry to calculate bonds, bond order, donor-acceptor interactions, and the distribution of electron density between atoms. The NBO also analysis the bonding in terms of the natural hybrid orbital. NBO calculations of title compounds were performed using NBO 3.1 program[31] as implemented in the Gaussian 09 package and a summary of important results is reported in Table 6. The higher the E(2) value, the stronger the interaction between electron donors and electron acceptors and reveals a more donating tendency from electron donors to electron acceptors and a greater degree of conjugation of the whole system. The possible selective intra-molecular hyper conjugative interactions noticed in BCPOT are

C2-C3→C4-C5 (20.38 Kcal/mol, π→π*),
C14 - S19→ C16-N18 (26.45 Kcal/mol, π→π*),
C16-N18→C15-O17 (25.72 Kcal/mol, π→π*),
C20-N25 → C20-H48 (27.97 Kcal/mol, σ→σ*),
C20-C37→ C20-N25 (23.45 Kcal/mol, σ→σ*),
C26-C27→C29-C33 (22.95 Kcal/mol, π→π*),
C28-C31→C26 -C27 (22.17 Kcal/mol, π→π*),
C38 - C40→ C37 - C39 (22.49 Kcal/mol, π→π*),
C38 - C40 → C42 - C44 (23.68 Kcal/mol, π→π*),
C42-C44→ C37 - C39 (28.45 Kcal/mol, π→π*),
C59-C60→ C62 - C65 (21.68 Kcal/mol, π→π*),
C61-C64→ C59 - C60 (22.21 Kcal/mol, π→π*),
C62-C65 →C61-C64 (22.54 Kcal/mol, π→π*)
with stabilization energies.

NCI surface analysis

The real space weak interaction, supported on electron density and derivatives is approached by RDG analysis and it is improved by Johnson *et al.*[32]. It is a dimensionless extent and the first gradient found in the literature. The leading intention of this portion is to study the non-covalent interactions between the dissimilar entities and to appraise their consequence in the steadiness of the crystal formation. The graphical visualization of non-covalent interaction locations is succeeded by NCI-RDG analysis. It is examined as resolve and helpful technique for characterizing repellent steric

Table 5 — Fukui function (fi+, fi-, Δf) for) of 1-benzyl-3-[2-(3-(4-chlorophenyl)-5-[4-(propan-2-yl)phenyl]-4,5-dihydro-1*H*-pyrazol-1-yl)-4-oxo-4,5-dihydro-1,3-thiazol-5(4*H*)-ylidene]-2,3-dihydro-1*H*-indol-2-one.

Atoms No.	Neutral (N)	Cation (N-1)	Anion (N+1)	f_k^+	f_k^-	$f_k°$	Δ*f*r	s_k^+	s_k^-	$s_k°$	ω_k^+	ω_k^-	$\omega_k°$
C1	-0.094	-0.082	-0.054	0.012	-0.040	-0.014	0.052	0.005	-0.016	-0.006	0.039	-0.132	-0.047
C2	0.197	0.185	0.102	-0.013	0.095	0.041	-0.108	-0.005	0.037	0.016	-0.041	0.312	0.135
C3	-0.255	-0.277	-0.111	-0.022	-0.144	-0.083	0.122	-0.008	-0.056	-0.032	-0.071	-0.472	-0.271
C4	-0.177	-0.220	-0.067	-0.043	-0.110	-0.076	0.067	-0.016	-0.042	-0.029	-0.140	-0.359	-0.249
C5	-0.226	-0.239	-0.107	-0.012	-0.120	-0.066	0.107	-0.005	-0.046	-0.025	-0.040	-0.391	-0.216
C6	-0.149	-0.182	-0.055	-0.032	-0.094	-0.063	0.062	-0.012	-0.036	-0.024	-0.105	-0.308	-0.207
C7	-0.033	-0.091	0.022	-0.058	-0.055	-0.056	-0.002	-0.022	-0.021	-0.022	-0.188	-0.180	-0.184
C8	0.614	0.587	0.313	-0.026	0.301	0.137	-0.327	-0.010	0.116	0.053	-0.087	0.984	0.449
H9	0.226	0.210	0.122	-0.016	0.104	0.044	-0.120	-0.006	0.040	0.017	-0.052	0.340	0.144
H10	0.219	0.202	0.120	-0.018	0.100	0.041	-0.117	-0.007	0.038	0.016	-0.058	0.326	0.134
H11	0.282	0.281	0.143	-0.002	0.140	0.069	-0.141	-0.001	0.054	0.027	-0.006	0.456	0.225
N12	-0.476	-0.496	-0.222	-0.019	-0.255	-0.137	0.235	-0.007	-0.098	-0.053	-0.064	-0.833	-0.448
O13	-0.706	-0.758	-0.337	-0.052	-0.368	-0.210	0.316	-0.020	-0.142	-0.081	-0.171	-1.205	-0.688
C14	-0.429	-0.466	-0.222	-0.037	-0.207	-0.122	0.170	-0.014	-0.080	-0.047	-0.120	-0.677	-0.398
C15	0.559	0.538	0.297	-0.021	0.262	0.120	-0.283	-0.008	0.101	0.046	-0.070	0.857	0.394
C16	0.051	0.031	0.048	-0.020	0.003	-0.008	-0.023	-0.008	0.001	-0.003	-0.065	0.011	-0.027
O17	-0.655	-0.714	-0.325	-0.058	-0.331	-0.195	0.273	-0.022	-0.127	-0.075	-0.190	-1.082	-0.636
N18	-0.559	-0.579	-0.286	-0.020	-0.273	-0.147	0.253	-0.008	-0.105	-0.057	-0.065	-0.894	-0.480
S19	0.801	0.796	0.407	-0.005	0.394	0.195	-0.399	-0.002	0.152	0.075	-0.015	1.289	0.637
C20	-0.108	-0.148	-0.209	-0.040	0.101	0.030	-0.141	-0.016	0.039	0.012	-0.132	0.329	0.099
N21	-0.228	-0.237	-0.074	-0.009	-0.154	-0.082	0.145	-0.004	-0.059	-0.031	-0.030	-0.504	-0.267
C22	-0.498	-0.485	-0.245	0.014	-0.253	-0.120	0.267	0.005	-0.098	-0.046	0.045	-0.828	-0.392
C23	0.281	0.190	0.093	-0.091	0.188	0.049	-0.279	-0.035	0.072	0.019	-0.298	0.615	0.159
H24	0.244	0.207	0.115	-0.038	0.129	0.046	-0.167	-0.014	0.050	0.018	-0.123	0.422	0.149
N25	-0.247	-0.268	-0.237	-0.021	-0.010	-0.016	-0.011	-0.008	-0.004	-0.006	-0.068	-0.034	-0.051
C26	-0.088	-0.070	-0.042	0.018	-0.047	-0.014	0.064	0.007	-0.018	-0.006	0.058	-0.152	-0.047
C27	-0.200	-0.228	-0.105	-0.028	-0.094	-0.061	0.066	-0.011	-0.036	-0.024	-0.092	-0.309	-0.200
C28	-0.165	-0.184	-0.091	-0.018	-0.075	-0.046	0.056	-0.007	-0.029	-0.018	-0.060	-0.244	-0.152
C29	-0.221	-0.230	-0.101	-0.008	-0.120	-0.064	0.112	-0.003	-0.046	-0.025	-0.027	-0.392	-0.210
H30	0.225	0.219	0.113	-0.005	0.111	0.053	-0.117	-0.002	0.043	0.020	-0.018	0.364	0.173
C31	-0.219	-0.231	-0.098	-0.012	-0.120	-0.066	0.108	-0.005	-0.046	-0.026	-0.040	-0.394	-0.217
H32	0.258	0.253	0.130	-0.005	0.128	0.061	-0.133	-0.002	0.049	0.024	-0.016	0.417	0.200
C33	-0.012	-0.041	-0.010	-0.028	-0.002	-0.015	-0.026	-0.011	-0.001	-0.006	-0.092	-0.008	-0.050
H34	0.242	0.228	0.126	-0.014	0.115	0.051	-0.129	-0.005	0.044	0.019	-0.046	0.377	0.165
H35	0.245	0.232	0.128	-0.013	0.118	0.052	-0.131	-0.005	0.045	0.020	-0.044	0.384	0.170
Cl36	-0.017	-0.058	0.007	-0.041	-0.024	-0.033	-0.017	-0.016	-0.009	-0.013	-0.135	-0.079	-0.107
C37	-0.094	-0.077	-0.052	0.017	-0.042	-0.012	0.059	0.007	-0.016	-0.005	0.056	-0.137	-0.040
C38	-0.168	-0.174	-0.093	-0.006	-0.075	-0.041	0.069	-0.002	-0.029	-0.016	-0.021	-0.247	-0.134
C39	-0.181	-0.182	-0.096	-0.001	-0.085	-0.043	0.084	0.000	-0.033	-0.017	-0.002	-0.278	-0.140
C40	-0.181	-0.188	-0.087	-0.007	-0.093	-0.050	0.087	-0.003	-0.036	-0.019	-0.022	-0.306	-0.164
H41	0.228	0.222	0.118	-0.006	0.110	0.052	-0.116	-0.002	0.042	0.020	-0.020	0.360	0.170
C42	-0.202	-0.210	-0.096	-0.007	-0.106	-0.057	0.099	-0.003	-0.041	-0.022	-0.023	-0.347	-0.185
H43	0.228	0.223	0.118	-0.005	0.111	0.053	-0.116	-0.002	0.043	0.020	-0.017	0.362	0.172
C44	0.024	0.004	0.020	-0.020	0.004	-0.008	-0.024	-0.008	0.001	-0.003	-0.065	0.013	-0.026
H45	0.228	0.215	0.120	-0.013	0.107	0.047	-0.120	-0.005	0.041	0.018	-0.042	0.351	0.155
H46	0.226	0.214	0.119	-0.012	0.106	0.047	-0.118	-0.005	0.041	0.018	-0.039	0.348	0.154
H47	0.248	0.213	0.118	-0.035	0.130	0.048	-0.165	-0.013	0.050	0.018	-0.114	0.425	0.156
H48	0.430	0.403	0.216	-0.027	0.213	0.093	-0.240	-0.010	0.082	0.036	-0.087	0.698	0.305
C49	-0.225	-0.221	-0.114	0.004	-0.110	-0.053	0.114	0.001	-0.043	-0.021	0.012	-0.361	-0.175
C50	-0.614	-0.615	-0.306	-0.001	-0.307	-0.154	0.306	-0.001	-0.118	-0.059	-0.005	-1.005	-0.505

(*Contd.*)

Table 5 — Fukui function (fi+, fi-, Δf) for) of 1-benzyl-3-[2-(3-(4-chlorophenyl)-5-[4-(propan-2-yl)phenyl]-4,5-dihydro-1*H*-pyrazol-1-yl)-4-oxo-4,5-dihydro-1,3-thiazol-5(4*H*)-ylidene]-2,3-dihydro-1*H*-indol-2-one.

Atoms No.	Neutral (N)	Cation (N-1)	Anion (N+1)	f_k^+	f_k^-	$f_k°$	Δ*f*r	s_k^+	s_k^-	$s_k°$	ω_k^+	ω_k^-	$\omega_k°$
H51	0.219	0.222	0.108	0.003	0.111	0.057	-0.108	0.001	0.043	0.022	0.010	0.363	0.186
H52	0.214	0.217	0.106	0.003	0.109	0.056	-0.106	0.001	0.042	0.021	0.009	0.355	0.182
H53	0.209	0.198	0.111	-0.012	0.099	0.044	-0.110	-0.004	0.038	0.017	-0.038	0.323	0.142
C54	-0.614	-0.616	-0.306	-0.002	-0.308	-0.155	0.306	-0.001	-0.119	-0.060	-0.006	-1.007	-0.507
H55	0.206	0.203	0.105	-0.003	0.101	0.049	-0.105	-0.001	0.039	0.019	-0.011	0.331	0.160
H56	0.209	0.206	0.106	-0.003	0.103	0.050	-0.106	-0.001	0.039	0.019	-0.010	0.335	0.163
H57	0.218	0.209	0.113	-0.009	0.105	0.048	-0.113	-0.003	0.040	0.018	-0.028	0.342	0.157
C58	-0.198	-0.196	-0.101	0.002	-0.097	-0.048	0.099	0.001	-0.037	-0.018	0.007	-0.318	-0.155
C59	-0.029	-0.014	-0.022	0.015	-0.007	0.004	0.022	0.006	-0.003	0.002	0.048	-0.023	0.013
C60	-0.210	-0.206	-0.108	0.004	-0.103	-0.049	0.107	0.002	-0.040	-0.019	0.014	-0.336	-0.161
C61	-0.246	-0.243	-0.125	0.003	-0.121	-0.059	0.124	0.001	-0.046	-0.023	0.010	-0.394	-0.192
C62	-0.200	-0.205	-0.097	-0.005	-0.103	-0.054	0.097	-0.002	-0.040	-0.021	-0.017	-0.336	-0.176
H63	0.227	0.229	0.113	0.002	0.114	0.058	-0.112	0.001	0.044	0.022	0.006	0.373	0.190
C64	-0.205	-0.210	-0.100	-0.005	-0.105	-0.055	0.100	-0.002	-0.041	-0.021	-0.017	-0.344	-0.181
C65	-0.213	-0.224	-0.101	-0.011	-0.112	-0.061	0.101	-0.004	-0.043	-0.024	-0.035	-0.366	-0.201
H66	0.224	0.217	0.116	-0.007	0.108	0.050	-0.115	-0.003	0.042	0.019	-0.024	0.353	0.165
H67	0.223	0.214	0.116	-0.009	0.107	0.049	-0.116	-0.003	0.041	0.019	-0.028	0.350	0.161
H68	0.216	0.205	0.114	-0.011	0.102	0.046	-0.113	-0.004	0.039	0.018	-0.035	0.334	0.150
H69	0.242	0.237	0.124	-0.005	0.118	0.057	-0.123	-0.002	0.046	0.022	-0.015	0.387	0.186
H70	0.223	0.221	0.112	-0.002	0.110	0.054	-0.112	-0.001	0.042	0.021	-0.006	0.361	0.177
H71	0.219	0.211	0.114	-0.009	0.105	0.048	-0.114	-0.003	0.041	0.019	-0.028	0.344	0.158
H72	0.223	0.221	0.113	-0.002	0.110	0.054	-0.113	-0.001	0.042	0.021	-0.008	0.361	0.176
H73	0.217	0.202	0.117	-0.015	0.100	0.042	-0.115	-0.006	0.039	0.016	-0.049	0.327	0.139

Table 6 — Second order perturbation theory analysis of Fock matrix in NBO basis corresponding to intra molecular bands of 1-benzyl-3-[2-(3-(4-chlorophenyl)-5-[4-(propan-2-yl)phenyl]-4,5-dihydro-1*H*-pyrazol-1-yl)-4-oxo-4,5-dihydro-1,3-thiazol-5(4*H*)-ylidene]-2,3-dihydro-1*H*-indol-2-one obtained B3LYP/6-31G (d, p) basis set.

Donor(i)	Type	ED/e	Acceptor(j)	Type	ED/e	E(2)[a] Kcal/mol	E(i)-E(j)[b]
σ	C1 - C2	1.95704	σ*	C7 - C14	6.68	1.04	0.074
π	C2 - C3	1.70534	LP (1)	C1	35.99	0.16	0.086
π	C2 - C3	1.70534	π*	C 4 - C5	20.38	0.31	0.071
σ	C3 - C4	1.97228	σ*	C2 - N12	8.28	1.01	0.082
σ	C3 - H9	1.97063	σ*	C1 - C2	6.13	1.01	0.070
π	C4 - C5	1.67742	LP*(1)	C6	48.73	0.16	0.094
π	C4 - C5	1.67742	π*	C2 - C3	19.33	0.28	0.066
σ	C5 - C6	1.97438	σ*	C1 - C7	6.97	1.14	0.080
σ	C6 - H11	1.96582	σ*	C1 - C2	7.16	0.97	0.075
π	C8 - O13	1.92528	LP (1)	C7	15.04	0.18	0.064
σ	C14 - S19	1.83808	σ*	C16 - N25	7.99	1.03	0.082
π	C14 - S19	1.83808	LP (1)	C7	9.96	0.27	0.062
π	C14 - S19	1.83808	π*	C15 - O17	14.82	0.35	0.072
π	C14 - S19	1.83808	π*	C16 - N18	26.45	0.32	0.096
π	C15 - O17	1.89199	π*	C14 - S19	10.69	0.23	0.053
σ	C15 - N18	1.96597	σ*	C7 - C14	7.35	1.14	0.082
σ	C15 - N18	1.96597	σ*	C16 - N25	9.56	0.91	0.084
π	C16 - N18	1.82179	π*	C14 - S19	17.44	0.27	0.072
π	C16 - N18	1.82179	π*	C15 - O17	25.72	0.28	0.085
σ	C16 - S19	1.97804	σ*	C7 - C14	6.44	1.28	0.082
σ	C20 - C22	1.93436	σ*	C16 - N25	8.07	0.87	0.075
σ	C20 - C22	1.93436	σ*	C20 - H48	6.22	0.95	0.069

(*Contd.*)

Table 6 — Second order perturbation theory analysis of Fock matrix in NBO basis corresponding to intra molecular bands of 1-benzyl-3-[2-(3-(4-chlorophenyl)-5-[4-(propan-2-yl)phenyl]-4,5-dihydro-1*H*-pyrazol-1-yl)-4-oxo-4,5-dihydro-1,3-thiazol-5(4*H*)-ylidene]-2,3-dihydro-1*H*-indol-2-one obtained B3LYP/6-31G (d, p) basis set. (*Contd.*)

Donor(i)	Type	ED/e	Acceptor(j)	Type	ED/e	E(2)[a] Kcal/mol	E(i)-E(j)[b]
σ	C20 - C22	1.93436	σ*	C23 - C26	7.28	1.06	0.079
σ	C20 - N25	1.90557	σ*	C20 - H48	12.34	0.47	0.104
σ	C20 - N25	1.90557	σ*	C20 - H48	27.97	0.96	0.148
π	C20 - N25	1.90557	π*	C16 - N18	9.86	0.38	0.059
π	C20 - N25	1.90557	σ*	C20 - N25	12.00	0.68	0.085
σ	C20 - C37	1.77522	π*	C20 - N25	23.45	0.81	0.130
σ	C20 - H48	1.23893	σ*	C20 - N25	13.81	0.48	0.085
σ	C20 - H48	1.23893	π*	C37 - C39	6.73	0.24	0.040
π	N21 - C23	1.97633	π*	C26 - C27	8.23	0.34	0.051
σ	C22 - H24	1.94170	π*	C20 - N25	6.20	0.76	0.068
σ	C22 - H24	1.94170	π*	N21 - C23	6.39	0.49	0.053
σ	C22 - H47	1.94375	π*	N21 - C23	6.35	0.49	0.053
π	C26 - C27	1.64238	π*	C28 - C31	20.19	0.30	0.071
π	C26 - C27	1.64238	π*	C29 - C33	22.95	0.28	0.072
π	C28 - C31	1.64997	π*	C26 - C27	22.17	0.28	0.071
σ	C28 - H32	1.97290	σ*	C26 - C27	6.20	1.05	0.072
π	C29 - C33	1.66996	π*	C26 - C27	19.33	0.30	0.069
π	C29 - C33	1.66996	π*	C28 - C31	19.67	0.31	0.071
σ	C37 - C38	1.96915	π*	C20 - N25	6.02	0.94	0.075
π	C37 - C39	1.97074	π*	C38 - C40	20.58	0.31	0.072
π	C37 - C39	1.97074	π*	C42 - C44	15.86	0.32	0.064
π	C38 - C40	1.63781	π*	C37 - C39	22.49	0.26	0.070
π	C38 - C40	1.63781	π*	C42 - C44	23.68	0.29	0.075
σ	C38 - H41	1.97624	σ*	C37 - C39	6.38	1.05	0.073
σ	C39 - H43	1.97568	σ*	C37 - C38	6.38	1.07	0.074
σ	C40 - H45	1.97536	σ*	C42 - C44	6.34	1.07	0.073
π	C42 - C44	1.61374	π*	C37 - C39	28.45	0.26	0.077
π	C42 - C44	1.61374	π*	C38 - C40	18.33	0.28	0.066
σ	C42 - H46	1.97556	σ*	C40 - C44	6.20	1.08	0.073
σ	C49 - H70	1.94278	σ*	C40 - C44	8.74	0.99	0.084
π	C59 - C60	1.97322	π*	C61 - C64	21.50	0.28	0.070
π	C59 - C60	1.97322	π*	C62 - C65	21.68	0.29	0.071
σ	C60 - H63	1.97597	σ*	C59 - C61	6.49	1.06	0.074
π	C61 - C64	1.66387	π*	C59 - C60	22.21	0.29	0.072
π	C61 - C64	1.66387	π*	C62 - C65	21.09	0.29	0.070
σ	C61 - H72	1.97640	σ*	C59 - C60	6.28	1.08	0.074
π	C62 - C65	1.65421	π*	C59 - C60	21.71	0.29	0.071
π	C62 - C65	1.65421	π*	C61 - C64	22.54	0.28	0.071

interaction van der Waals interactions and hydrogen bonds using a simple colour code. The quality of the strength of the interaction can be investigated through RDG surface analysis. Red, green and blue colour codes are used to describe destabilizing steric interactions, van der Waals, and stabilizing hydrogen bonding respectively.

$$RDG(r) = \frac{1}{2(3\pi r^2)^{1/2}} \frac{|\nabla \rho(r)|}{\rho(r)^{4/3}} \quad \ldots (5)$$

The plot of r(r) against the l2 sign will help to comprehend the quality and strength of the interaction. The sign of l2, the second greatest value of the Hessian matrix of electron density, is used to find the nature of an interaction. If l2 > 0, for non bonded and if l2 < 0 for bonded. The RDG isosurface of the title compound was drawn with an isosurface value of 0.5 as illustrated in Fig. 7. The software and it was plotted by Multiwfn and VMD program[33]. The red colour in scale in the figure depicts a forcible

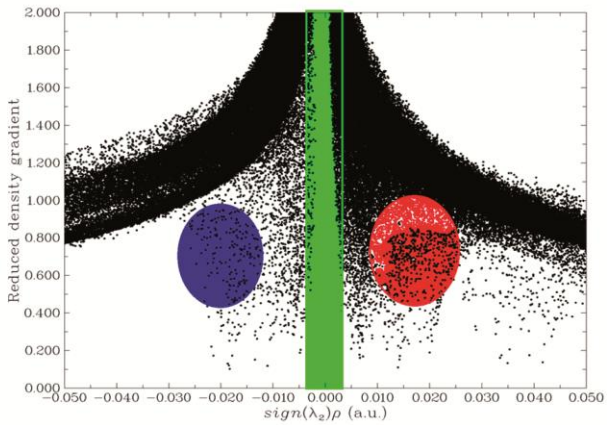

Fig. 7 — NCI surface analysis 2D of BCPOT.

repulsion that seems in all centralized in the ring system. While a strong van der Waals interaction took place between the amide group and one of the propane phenyl as well as one hydrogen atom in the chloro substituted phenyl ring.

ELF and LOL analysis

The ELF (electron localization function) and LOL (localized orbital locator) maps were topology analysis performed based on the covalent bonds. These maps reveal the regions where the probability of finding an electron pair is high[34]. ELF and LOL share a similar interpretation depending on the kinetic energy density[35]. Colour shade maps of the ELF and LOL for the title molecule were presented in Figs 8(a) and 8(b), respectively. The electron localization function is the estimation of electron localization in atomic and molecule systems[36]. Pauli repulsion existing among two like–spin electrons was used as a measure of electron localization. The region with the strongest Pauli repulsion corresponds to highly localized electrons. ELF studies describe the bonding, reactivity, and chemical structure[37]. The upper limit for ELF is 0.8 and the lower limit is 0. Two-dimensional graphical data employing colour gradiation is used to characterize the ELF values for the title compound. Red colour corresponds to high values of ELF while blue represents the region with a low end of ELF value. For the title compound, the maximum Pauli repulsion was around hydrogen with a single electron depicted by the red region around H9, H10, H11, H24, H30, H32, H34, H35, H41, H43, H45, H46, H47, H48, H51, H52, H53, H55, H56, H57, H63, H66, H67, H68, H69, H71, H72, and H73. The regions with chlorine nitrogen having similar spin electrons close together were depicted by the blue

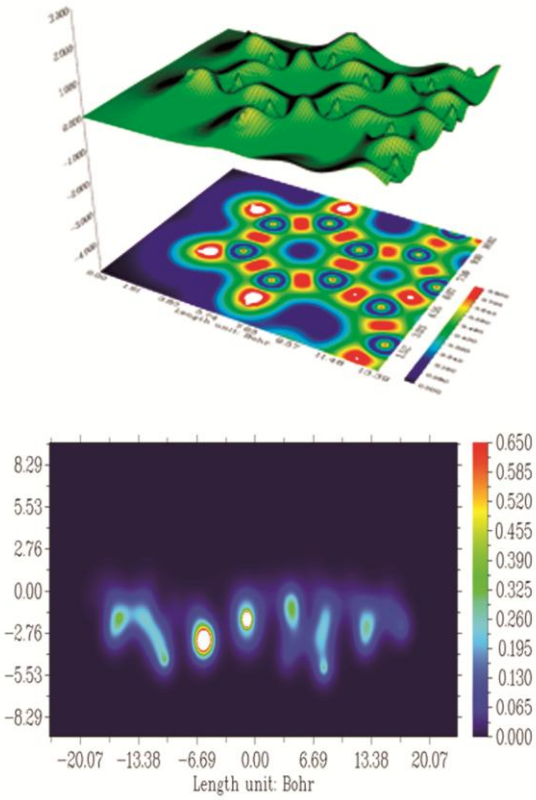

Fig. 8 — (a) ELF and (b) LOL of BCPOT.

region, whereas electron depletion regions (blue regions) are identified at N12, O13, O17, N18, S19, N21, N25, and Cl36. ELF and LOL analysis describes the chemical structure, molecular bonding, and reactivity with extensive prominence in their use for the quantitative analysis of aromaticity.

Molecular docking study

The protein-drug interaction was studied by automated docking to determine the orientation of inhibitors bound to the active site of the target protein. A genetic algorithm method, implemented in the program Autodock 4.2 was employed[9]. The 2D structures (.mol) of the BCPOT are converted to 3D structures (PDB). The protein structure file was downloaded from the protein data bank[38] and was edited by removing the hetero atoms and adding C-terminal oxygen. For docking calculations, Gasteinger partial charges were assigned to the inhibitors and non-polar hydrogen atoms were assigned to the inhibitors and non-polar hydrogen atoms were merged. All torsions were allowed to rotate during docking. The grid map was centered on the residues of the protein. The number of docking runs was 50,

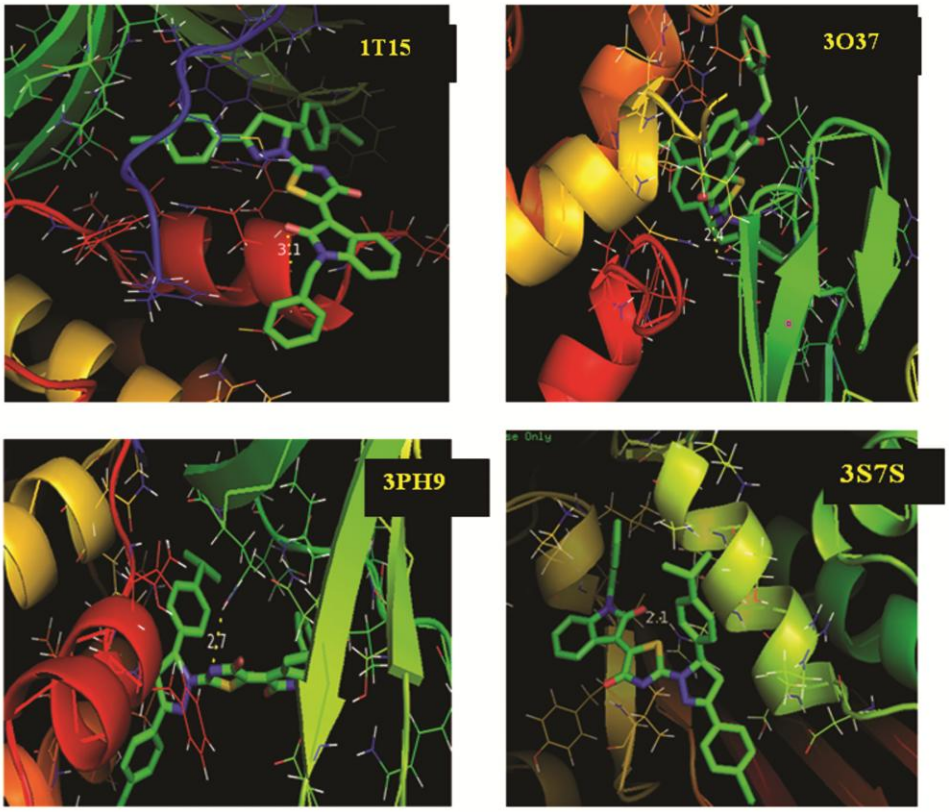

Fig. 9 — BCPOT docked into the binding site of anticancer proteins.

the population in the genetic algorithm was 250, and the number of energy evaluations was 1000. The docking results for inhibitors against protein, showed minimum docking energy, inhibition constant, with RMSD as noted. The molecular docking of the protein with BCPOT yielded the best possible conformations with parameters including the docking energy, binding energy, intermolecular energy, inhibition constant, and RMSD (Table 7). Molecular docking studies were performed using Auto dock tool software[39]. The target protein from anticancer activity drugs against breast cancer was downloaded from

Protein data

Bank (PDB ID: 1T15, 3O37, 3PH9, 3S7S) and the active site were chosen. A molecular docking study was carried out for the title compound. Figure 9 shows the active site of the three-dimensional structure of a target receptor molecule protein. Among the all active sites, the pocket found to be the best active contains 58 amino acids. The minimum docking energy was found in the 1T15-ligand -10.17 Kcal/mol) and RMSD (root mean square deviation) 72.294 Å, and estimation inhibition constant of 35.31 nm. The minimum docking energy was found in the 3O37-ligand -9.12 Kcal/mol) and RMSD (root mean square deviation) 63.146 Å, and estimation inhibition constant of 205.28 nm. The minimum docking energy was found in the 3PH9 –ligand (-11.46 Kcal/mol) and RMSD (root mean square deviation) 65.494 Å, and the estimation inhibition constant of 3.99 nm. The minimum docking energy was found in the 3S7S -ligand (-9.22 Kcal/mol) and RMSD (root mean square deviation) 41.114 Å, and the estimation inhibition constant of 175.04 nm.

Table 7 — Binding affinity for docking of 1-Benzyl-3-[2-(3-(4-chlorophenyl)-5-[4-(propan-2-yl)phenyl]-4,5-dihydro-1*H*-pyrazol-1-yl)-4-oxo-4,5-dihydro-1,3-thiazol-5(4*H*)-ylidene]-2,3-dihydro-1*H*-indol-2-one

Protein name	PDB ID	Bond Length (Å)	Amino acid	Binding energy (kcal/mol)	Inhibition constant (nM)	RMSD (Å)
Anticancer	1T15	3.1	GLN A 299	-10.17	35.31	72.294
	3O37	2.4	GLN A 110	-9.12	205.28	63.146
	3PH9	2.7	GLN A 110	-11.46	3.99	65.494
	3S7S	2.1	HIS A 1652	-9.22	175.04	41.114

Conclusion

The examination of the present work has enlightened the spectroscopic properties such as optimized geometrical parameters, vibrational assignments, and electrical properties of the title compound by applying FTIR and FT-Raman title molecule revealing the necessary techniques and theoretical studies done by the density functional theory. The comparative influence associated with experimental and theoretical knowledge gives a full description of the vibrational assignments of the title molecule. The charge transfer occurs in the molecule between HOMO and LUMO energies, and the frontier energy gap is calculated. The band gap energy of HOMO-LUMO is -3.21eV. The molecular electrostatic potential diagram of the title molecule revealed the negative and positive regions. Fukui function helps to identify the electrophilic and nucleophilic nature of the title molecule. The molecular docking study shows that the lowest binding energy for the title compound with the protein is -11.46 Kcal/mol.

References

1 Davide Romani & Silvia Antonia Brand, *Int J Soc Res Methodol*, 8 (2017) 66.
2 Ladetto María F, Arquez María J M, Romani Davide & Brand Silvia A, *J Adv Chem*, 16 (2019) 6325.
3 VijiA, Balachandran V, Babiyana S & Narayana B, *J Mol Struc*, 1203 (2020) 127452.
4 VijiA, Balachandran V, Babiyana S, Narayana B & Salian Vinutha V, *J Mol Struc*, 1215 (2020) 128244.
5 Salian Vinutha V, Narayana Badiadka, Sarojini Balladka K, Kumar Madan S, Nagananda Govinahalli S, Byrappa Kullaiah & Kudva Avinash K, *Spectrochim Acta*, 174 (2017) 254.
6 Frisch M J, Trucks G W, Schkegel H B, Scuseria G C, Robb M A, Cheeseman J R, Scalmani G, Barone V, Mennucci B, Bloino G A, Zheng G, Sonnenberg J L, Hada M, Ehara M, Toyota K, Fukuda R, Hasegawa J, Ishida M, Nakajima T, Honda Y, Kitao O, Nakai H, Vreven T, Montgomery J A, Peralta J E, Ogliaro F, Bearpark M, Heyd J J, Brothers E, Kudin K N, Staroverov V N, Keith T, Kobayashi R, Normand J, Rghavachri K, Rendell A, Burant J C, Iyengar S S, Tomasi J, Cossi M, Rega N, Millam J M, Klene M, Knox J E, Cross J B, Bakken V, Adamo C, Jaramillo J, Gomperts R, Stratmann R E, Yazyev O, Austin A J, Cammi R, Pomelli C, Ochterski J W, Martin R L, Morokuma K, Zakrzewski V G, Voth G A, Salvador P, Dannenberg J J,.Dapprich S, Daniels A D, Farkas O, Foresman J B, Ortiz J V, Cioslowski J, Fox D J, *Gaussian Inc, Wallingford CT, Gaussian 09, Revision D.01*, (2013).
7 Varghese H T, Panicker C Y & Philip D, *J Raman Spect*, 38 (2007) 309.
8 Lu T & Chen F, *J Comput Chem*, 33 (2012) 580.
9 Morris G M, Huey R, Lindstrom W, Sanner M F, Belew R K, Goodsell D S & Olson A J, *J Comput Chem*, 30 (2009) 2785.
10 Sheena Mary Y, Tresa Varghese Hema, Panicker C Y, Thiemann T, Al Saadi Saheeed Abdulaziz, Popoola A, Van Alsenoy C & Al Jasem Yosef, *Spectrochim Acta A*, 150 (2015) 533.
11 Erdogu Y, Tahir Gulluoolu M & Yurdakul S, *J Mol Struct*, 889 (2008) 361.
12 Ditchfield R, *J Chem Phys*, 56 (1972) 5688.
13 Hernandez O, Knight K S, Van Beek W, Boucekkine A, Boudjada A, Paulus W & Meinnel J, *J Mol Struct*, 791 (2006) 41.
14 Fatma S, Bishnoi A, Singh V, Al-Omary F A M, El-Emam A A, Pathak S, Srivastava R, Prasad O & Sinha L, *J Mol Struct*, 1110 (2016) 128.
15 Smith B, *Infrared spectral interpretation*, CRC Press, Boca Raton, (1999).
16 Durig J R, Little T S, Gounev T K, Gardner J K & Sullivan J F, *J Mol Struct*, 375 (1996) 83.
17 Kundoo S, Banarjee A N, Saha P & Chattopadhyaya K K, *Mater Lett*, 57 (2003) 2193.
18 Wattanathana W, Nootsuwan N, Veranitisagul C, Koonsaeng N, Suramitr S, Laobuthee A, Murugavel S, Sundaramoorthy S, Lakshmanan D, Subahashini R & Pavan Kumar P, *J Mol Struct*, 1131 (2017) 51.
19 Bellamy L J, Third Ed., Chapman and Halls, London, (1975).
20 Hiremath C S & Sundius T, *Spectrochim Acta A*, 74 (2009) 1260.
21 Silverstein R M, Webster F X & Kiemle D, *Spectrometric identification of organic compounds*, 2nd edn, (John-Wiley & Sons Inc.), 2005.
22 Almutairi M S, Alanazi A M, Al-Abdullah E S, El-Emam A A, Pathak S K, Srivastava R, Prasad O & Sinha L, *Spectrochim Acta A Mol Biomol Spectrosc*, 140 (2015) 1.
23 Fliszar S, *Charge Distributions and Chemical Effects*, (Springer, New York), 1983.
24 Sponer J & Hobza P, *Int J Quantum Chem*, 57 (1996) 959.
25 Murry J S & Sen K, *Molecular Electrostatic Potential Concepts and Applications*, (Elsevier, Amesterdam), 1996.
26 Shoba D, Periandy S, Boomadevi S & Fereduni E, *Spectrochim Acta A*, 118 (2014) 438.
27 Edwin B, Amalanathan M & Hubert Joe I, *Spectrochim Acta A*, 96 (2012) 10.
28 Singh R N, Tiwari Kumar A, Rawat P, Baboo V & Divya Verma R K, *Spectrochim Acta A*, 92 (2012) 295.
29 Raveendran P R, Menon V V, Shyma M Y, Armakovic S, Armakovic S J & Panicker C Y, *J Mol Struct*, 1130 (2017) 208.
30 Morell C, Grand A & Toro-Labbe A, *J Phys Chem A*, 109 (2005) 205.
31 Aruldas D, Hubert Joe I, Roy S D D & Balachandran S, *Spectrochim Acta A*, 108 (2013) 89.
32 Johnson E R, Keinan S, Mori-Sanchez P, Contreras-Garcia J, Cohen A J & Yang W, *J Am Chem Soc*, 132 (2010) 6498.
33 Humphray W, Dalke A & Schulten K, *J Mol Graph*, 14 (1996) 33.
34 Silvi B & Savin A, *Nature*, 371 (1994) 683.
35 Jacobsen H, *Can J Chem*, 86 (2008) 695.
36 Becke A D & Edgecombe K E, *J Chem Phys*, 92 (1990) 5397.
37 Poater J, Duran M, Sola M & Silvi B, *Chem Rev*, 105 (2005) 3911.
38 RCSB protein data bank (http://www.rcsb.org/pdb/home/home.do)
39 Viji A, Revathi B, Balachandran V, Babiyana S, Narayana B & Salian Vinutha V, *Chem Data Collect*, 30 (2020) 100585.